Title:

Deciphering the roles of cell shape and Fat and Dachsous planar polarity in arranging the *Drosophila* apical microtubule network through quantitative image analysis

Authors and affiliations:

Miguel Ramírez Moreno[1,2,3], Robert Hunton[1], David Strutt[1]*, Natalia A. Bulgakova[1,2]*

[1]School of Biosciences, University of Sheffield, Sheffield S10 2TN, UK

[2]Bateson Centre, University of Sheffield, Sheffield S10 2TN, UK

[3]Present address: School of Biological Sciences, University of Southampton, SO17 1BJ, UK

*Corresponding authors: n.bulgakova@sheffield.ac.uk, d.strutt@sheffield.ac.uk

Running head:

Apical microtubule network organisation

Keywords:

Microtubules, Ft-Ds, Fat-Dachsous, Planar Polarity, PCP, Cell shape, *Drosophila*

Abstract

In epithelial cells, planar polarisation of subapical microtubule networks is thought to be important for both breaking cellular symmetry and maintaining the resulting cellular polarity. Studies in the *Drosophila* pupal wing and other tissues have suggested two alternative mechanisms for specifying network polarity. On one hand mechanical strain and/or cell shape have been implicated as key determinants, on the other the Fat-Dachsous planar polarity pathway has been suggested to be the primary polarising cue. Using quantitative image analysis in the pupal wing, we reassess these models. We found that cell shape was a strong predictor of microtubule organisation in the developing wing epithelium. Conversely Fat-Dachsous polarity cues do not play any direct role in the organisation of the subapical microtubule network, despite being able to weakly recruit the microtubule minus-end capping protein Patronin to cell boundaries. We conclude that any effect of Fat-Dachsous on microtubule polarity is likely to be indirect, via their known ability to regulate cell shape.

Introduction

The polarity of epithelial cells is essential for their correct function within tissues. There are two principal types of cell polarity – apicobasal and planar, the latter describing the coordinated polarisation of cells within the plane of cell sheets (Goodrich and Strutt, 2011; Butler and Wallingford, 2017). One of the manifestations of such polarities is the asymmetry of cytoskeletons such as the microtubule cytoskeleton. Microtubules are polar filaments with highly dynamic plus ends and more stable minus ends. Their preferential directionality within cells leads to biased trafficking of molecules to specific locations by motor proteins moving along individual microtubule filaments (Hirokawa and Takemura, 2005; van Haren and Wittmann, 2019; Masucci *et al.*, 2022). As a result, such directionality of the microtubule cytoskeleton can play roles in both the initial breaking of cellular symmetry as well as the maintenance of polarity once it is established (Shimada *et al.*, 2006; Siegrist and Doe, 2007; Bulgakova *et al.*, 2013; Matis *et al.*, 2014). Many epithelial cells have two microtubule systems with distinct organisations – an apicobasal array with microtubule plus ends pointing basally, and a dense network beneath (and parallel to) the apical surface known as the "subapical network" (Figure 1A) (Toya and Takeichi, 2016; Akhmanova and Kapitein, 2022).

The subapical microtubule network contributes to both morphogenesis and function of epithelia, including such diverse roles as the regulation of cell morphology and adhesion,

planar polarity, and positioning of cilia and their coordinated beating (Vladar *et al.*, 2012; Gomez *et al.*, 2016; Herawati *et al.*, 2016; Tateishi *et al.*, 2017; Kimura *et al.*, 2021; Akhmanova and Kapitein, 2022). However, it is unclear what determines the correct organisation of subapical microtubule networks and two competing models have been proposed.

The first model suggests that the microtubules follow the physical constraints set up by mechanical strain (Chien *et al.*, 2015) or by cell shape (Gomez *et al.*, 2016). As a result, the more cells are elongated in the tissue plane, the higher the alignment of microtubules with each other within the subapical network – the overall direction being aligned with the cell's long axis (Figure 1A) (Gomez *et al.*, 2016). This cell shape-driven microtubule alignment has been shown to be robust in several epithelia, including the *Drosophila* pupal wing epithelium (Płochocka *et al.*, 2021). It was further proposed that the degree of microtubule alignment but not the overall direction might be affected by the positioning of microtubule minus ends (Płochocka *et al.*, 2021).

The second model suggests that the organisation of the subapical network is actively controlled by planar polarity machinery. Planar polarity (also known as planar cell polarity, PCP) is established and maintained by two widely-studied systems in animal cells; the "core" Frizzled-dependent pathway and the Fat-Dachsous (Ft-Ds) pathway (Devenport, 2014; Hale *et al.*, 2015). Both pathways rely on the heterophilic binding of membrane proteins that are distributed asymmetrically across the tissue plane in response to upstream patterning signals such as morphogen gradients (Figure 1B) (Lawrence and Casal, 2018). In both invertebrates and vertebrates, there is evidence that these pathways can specify planar polarity on either the same or different axes within a single tissue depending on the context (Merkel *et al.*, 2014; Zakaria *et al.*, 2014; Vu *et al.*, 2019) (reviewed in Strutt and Strutt, 2021).

Microtubule polarity has been proposed to be regulated by both the core planar polarity pathway in vertebrates (Sepich *et al.*, 2011; Vladar *et al.*, 2012; Chien *et al.*, 2015) and by the Ft-Ds pathway in both vertebrates and flies (Harumoto *et al.*, 2010; Li-Villarreal *et al.*, 2015). Specifically, in the *Drosophila* pupal wing, it has been proposed that the Ft-Ds pathway controls the orientation of microtubules within the subapical network along the proximodistal axis, and this provides a polarity cue for the core pathway through the polarised transport of core proteins towards microtubule plus ends at distal cell edges (Shimada *et al.*, 2006; Harumoto *et al.*, 2010; Matis *et al.*, 2014; Olofsson *et al.*, 2014) (reviewed in Strutt and Strutt, 2021). Finally, both cell elongation due to mechanical strain,

and the core planar polarity pathway, have been shown to cooperate in apical microtubule alignment during *Xenopus* gastrulation (Chien *et al.*, 2015).

Currently, it is unclear if the Ft-Ds pathway affects the organisation of the subapical microtubule network directly or indirectly. In the pupal wing, minus ends of the subapical microtubules are localised at apical junctions in a polarised manner thought to align with Ft-Ds planar polarity (Matis *et al.*, 2014), and Ft-Ds are suggested to be required for the association between the subapical microtubules and Adherens Junctions (Singh *et al.*, 2018). From this, it has been inferred that Ft-Ds may play a direct role in capturing or nucleating microtubules, although the molecular link between Ft-Ds and microtubules is unknown. At the same time, Ft-Ds might act indirectly on the subapical microtubule network, as there is evidence that they alter cell shape, and in particular cell elongation, by polarising the distribution of the atypical myosin Dachs (Aigouy *et al.*, 2010; Mao *et al.*, 2011; Bosveld *et al.*, 2012).

Here, we reassess the evidence for these models of how the subapical microtubule network is organised, looking in the *Drosophila* pupal wing epithelium due to the wealth of acquired knowledge about this system. We have developed a robust pipeline of work where automated image analysis has allowed us to determine characteristics on a cell-by-cell basis (Figure 1C). Similar approaches have been used previously for linking planar polarity and cell orientation (Hirano *et al.*, 2022), but our pipeline introduces microtubule analysis. We identified two regions within pupal wings with distinct relationships between the orientation of cell shape and Ft-Ds polarity, allowing us to uncouple their effects on the organisation of subapical microtubule networks. Studying these two regions in wings with normal and altered Ft-Ds function revealed that the Ft-Ds complexes weakly promote localisation of the microtubule minus-end capping protein Patronin. Despite this, we found that Ft-Ds polarity cues do not play any substantial role in the subapical microtubule network organisation in the developing wing epithelium. Conversely, cell shape was a strong predictor of microtubule organisation. Altogether, our findings reconcile the two models of the subapical microtubule network organisation, by placing cell shape as the primary cue, which might be regulated upstream by Ft-Ds planar polarity in a context-dependent manner.

4

Results

Divergent axes of Ft-Ds polarity and cell elongation in the pupal wing

To start disentangling the relationship between the Ft-Ds pathway, cell shape and subapical microtubule organisation using automated image analysis, we first quantified the polarity of Ft-Ds in different regions of the pupal wing using our established tool based on Principle Component Analysis (PCA) (Tan *et al.*, 2021). Previous reports have come to conflicting conclusions regarding Ft-Ds polarity in the developing wing; Matis *et al.* (2014) have reported that polarity is proximodistally oriented at 24h after puparium formation (APF) when microtubules are also aligned proximodistally following the long axis of the cells (Shimada *et al.*, 2006; Harumoto *et al.*, 2010; Matis *et al.*, 2014; Płochocka *et al.*, 2021). Conversely, Merkel *et al.* (2014) observed a primarily radial/anteroposterior orientation of Ft-Ds polarity throughout most of the wing at this stage (Merkel *et al.*, 2014).

We focused our analysis on two regions which show large discrepancies in the published reports, the distal region of the wing between veins 3 and 4 and the posterior region below vein 4 (v4) at 24h APF (Figures 1C and 2A). Coarse grain analysis of Ds-EGFP polarity showed a radial/anteroposterior pattern across these regions (Figure 2A), consistent with the previous observations of Merkel *et al* (2014). We used our analysis pipeline to map both cell orientation and Ds polarity at a single-cell resolution (Figure 2B, see Materials and Methods). To assess the cell shape polarity – the direction, in which cells are elongated within the tissue – we measured cell angles (directions of long axes) of individual cells in both regions (Figure 1C, see Materials and Methods). Cells from both regions exhibited strong similar magnitudes of Ds polarity as assessed by our PCA method (Figure 2C). At the same time, the cells below v4 (posterior) were more elongated than those above v4 (distal) based on the distributions of their eccentricities (Figure 2D).

To explore the relationship between cell shape and Ds polarities and directly compare the two regions of the pupal wing, we plotted both cell and Ds polarity angles relative to the average cell angle in each region/wing (Figure 2E). The normalisation of cell orientation to the average orientation angle demonstrated the high cellular coordination with many cells elongating in the same direction, which is more apparent in the posterior region, potentially due to the higher eccentricities of individual cells (Figures 2D-E). Next, we calculated the percentage of cell and of Ds polarity angles that fell into the quadrant with the most cell angles (i.e. 0±45°) (Harumoto *et al.*, 2010) (Figure 2E-F). This revealed that cell orientation

5

and Ds polarity were similar in the distal compartment but significantly differed in the posterior (Figure 2F). Therefore, these data demonstrate an uncoupling between cell orientation and Ds polarity in the posterior region below v4, but not in the distal region of the wing. Thus, we found distinct relationships between cell shape and Ft-Ds polarities depending on the region of the pupal wing. Such an uncoupling in the posterior region indicates that the mechanisms that determine Ft-Ds polarity and cellular elongation within a tissue are, at least partially, independent. Importantly, the differences between cell shape and Ds polarities in these regions allow us to investigate the effect of both factors on the organisation of the subapical microtubule network.

Microtubule organisation correlates with cell shape orientation but not Ft-Ds polarity
Both Ft-Ds and subapical microtubules are positioned within subapical domains of pupal wing cells (Ma *et al.*, 2003; Shimada *et al.*, 2006; Silva *et al.*, 2006; Harumoto *et al.*, 2010; Matis *et al.*, 2014; Gomez *et al.*, 2016; Płochocka *et al.*, 2021). Therefore, we next employed high-resolution imaging (~120 nm in XY and ~350 nm in Z directions) (Wu and Hammer, 2021) to ask whether the subcellular localisations of Ft-Ds and microtubules were consistent with the model whereby Ft-Ds capture microtubules. In the wing, the Ft-Ds complexes localise in "puncta" – discrete accumulations of stable clustered Ft-Ds complexes (Hale *et al.*, 2015). The fixation conditions required to image microtubules (see Materials and Methods) were compatible with the preservation of Ds-EGFP puncta (Figure 3A). Intensity profiles along the apicobasal cell axis showed that Ds-EGFP was indeed found in the same apicobasal plane as the subapical microtubules in both distal and posterior regions (Figure 3B, C), consistent with the possibility that the Ft-Ds complexes directly affect microtubules.

Therefore, we next explored the model that the Ft-Ds complexes capture microtubules. To this end, we used automated image analysis to determine whether there was a correlation between the planar polarised localisation of Ds-EGFP puncta and local increases in the density of microtubules in the two regions of interest of the pupal wing (Figure 4A, B, see Materials and Methods). We compared levels of the tubulin signal within the Ds-EGFP puncta and in the direct vicinity of these puncta ("puncta halo") to those within non-puncta regions of the cell boundaries – regions that are largely depleted for Ds-EGFP – and in their vicinity ("non-puncta halo"), and in the cytoplasm (Figure 4A). As expected, Ds-EGFP was predominantly found in puncta and depleted from other cellular areas in both pupal wing regions (Figure 4B, C, E). We did not observe an enriched accumulation of tubulin signal in the vicinity of the Ds-EGFP puncta in either pupal wing region (Figure 4B, D, F). Thus, there

6

are no detectable local changes in microtubule density depending on Ft-Ds concentrations, making it unlikely that Ft-Ds complexes directly capture or cluster microtubules.

Next, we asked if Ft-Ds affect the overall organisation of subapical microtubules, by testing whether it is the Ft-Ds distribution or cell shape that best correlates with the following two aspects of microtubule organisation: the relative alignment of microtubules with each other and the overall direction of the whole subapical network (Figure 1A). We examined these two aspects in individual cells in both distal and posterior regions of pupal wings (Figure 5A), in relation to Ft-Ds polarity and cell elongation.

The microtubule angle distribution represents how well the microtubules are aligned with each other within individual cells (Figure 5B) and can be expressed as the Microtubule Standard Deviation (MTSD) – the standard deviation of the best-fit von Mises distribution reflecting the width of the peak (Gomez *et al.*, 2016). MTSD correlated with cell elongation (Figure 5C) – more elongated cells with higher eccentricities had a steeper distribution (smaller MTSD) that reflected more aligned microtubules, with no significant difference between the two regions of the pupal wing examined. Such correlation of the microtubule angle distribution with the cell eccentricity agrees with the reported robustness of microtubule alignment with each other in subapical microtubule networks of epithelial cells (Płochocka *et al.*, 2021).

At the same time, we found that the overall microtubule network direction aligned with the axis of cell orientation (Figure 5E-F), with an uncoupling from Ds polarity in the posterior region of the developing wing. Additionally, we observed a better alignment of microtubule networks with the orientation of the cells in the posterior region (Figure 5E-F), which are more elongated than those in the distal region (Figure 5D). Therefore, we conclude that the direction of the microtubule network inside cells depends on the angle of the cell elongation axis, an effect which is particularly strong in the posterior region, rather than Ft-Ds polarity.

Ft-Ds junctional complexes promote localisation of the microtubule minus-end binding protein Patronin

Our findings support the overall organisation of the subapical microtubule network being robust and depending on the cell shape rather than the distribution of the Ft-Ds complexes. However, they do not exclude changes to the detail of this organisation dependent on Ft-Ds activity. The localisation of the minus ends in non-centrosomal networks is of particular

interest, as it ensures the correct polarised transport by motor proteins (Steinhauer and Kalderon, 2006; Zhelezov *et al.*, 2019).To examine the possibility that Ft-Ds complexes alter the distribution of the minus ends without affecting the overall organisation of subapical microtubules, we turned to the minus-end capping protein Patronin which localises at apical junctions and exhibits an asymmetrical distribution in the *Drosophila* embryonic epidermis that depends on the cell elongation (Goodwin and Vale, 2010; Płochocka *et al.*, 2021).

Patronin-GFP was also enriched at the cell junctions in the pupal wing (Figure 6A). There were no differences in the average levels of Patronin-GFP at the cell boundaries between distal and posterior regions (Figure 6B). When its distribution was assessed using PCA, Patronin-GFP appeared to be uniformly distributed along cell boundaries, with the average polarity being lower than that of E-cadherin (Figure 6C-D). However, we found that there were slightly higher levels of Patronin-GFP within Ds puncta along the cell boundaries in both distal and posterior regions of pupal wings (Figure 6E-H). This suggests that the Ft-Ds complexes might capture microtubule minus ends associated with Patronin. To strengthen this conclusion, we correlated the intensity of Ds and Patronin-GFP on a puncta-by-puncta basis. We find a mild but significant correlation in both distal and posterior regions – 0.06 (p = 0.0002) and 0.09 (p < 0.0001), respectively. This correlation supports the possibility that Ft-Ds complexes could affect subapical microtubule networks via regulation of Patronin localisation. Additionally, this highlights the limitations of using the PCA analysis alone – the moderate increase of Patronin-GFP levels within polarised Ds puncta appears to be below its sensitivity to detect polarisation at the cell level, probably due to the high levels of unpolarised Patronin-GFP outside of Ds puncta.

To further investigate the relationship between Ft-Ds and Patronin, we sought to genetically target the Ft-Ds pathway and determine the resulting effects on Patronin localisation. Therefore, we disrupted Ft-Ds polarity by temporally inducing Ds overexpression in the posterior compartment of the wing using a *hedgehog*-Gal4 driver. In this condition, cells in posterior regions overexpress Ds, whereas only cells in the posterior half of the distal regions do, providing an internal control in nearby anterior tissue. The induction from 18h APF led to an increase in Ds levels at 24h APF accompanied by reduced Ds polarity in overexpressing posterior and distal regions (Figures 6I-J). Concomitantly, the polarity of Ds increased in the adjacent distal internal control cells with unmodified Ds levels (Figure 6J), likely due to the non-autonomous propagation of polarity from the overexpression region (Brittle *et al.*, 2012).

8

We found that neither reduced Ds polarity in the cells that overexpress Ds nor increased Ds polarity in their neighbours (distal internal control region) were accompanied by changes in Patronin-GFP polarities (Figure 6J). However, as shown above, the PCA method is not powerful for detecting the correlation between Ds and Patronin localisation. To further examine the interaction between Ds and Patronin-GFP and the consequences of Ds overexpression on its distribution, we next measured the average levels of Patronin-GFP localised at cell boundaries (as there were no apparent Ds puncta when Ds was overexpressed, Figure 6I). Ds overexpression increased the levels of Patronin-GFP at the cell boundaries in both regions, whereas it was not significantly affected in the internal control with normal Ds levels (Figure 6K). This finding supports the recruitment of Patronin to cell boundaries and the potential capture of microtubule minus ends by the Ft-Ds complexes.

Experimental manipulation of Ft-Ds planar polarity does not reorganise microtubules

The observed uncoupling of Ft-Ds polarity and microtubule organisation in the posterior region suggested that during normal development Ft-Ds are unlikely to override the effects of cell shape on microtubule network organisation despite potential effects on the distribution of microtubule minus ends via Patronin. Consistent with this, we found that Ds overexpression did not change the alignment of microtubules with each other in the two wing regions (Figure 7A-B). The correlation between MTSD and cell eccentricity remained unchanged in both regions when comparing normal and elevated levels of Ds (Figure 7C). Note that Ds overexpression had a mild effect on cell shape as in the distal region cells with excess Ds were more elongated (Figure 7D), demonstrating that the Ft-Ds pathway can contribute to shaping cells in the pupal wing. Overall microtubule network directions remained aligned with cell angles, regardless of the disrupted Ds polarity produced by the protein overexpression (Figure 7E-F). Notably, the increase in cell eccentricity distally appeared to increase both the coordination of cell alignment with each other and the alignment of microtubule angles with cell angles (Figure 7E), in agreement with what we observed in pupal wings with unaltered Ft-Ds pathway (Figure 5E-F), supporting the primary role of cell shape in organising the subapical microtubule network.

Finally, we disrupted Ft-Ds polarity by removing Ds using the strong loss-of-function ds^{UA071} allele and FRT-mediated mitotic recombination with an *arm-LacZ* transgene on the homologous chromosome to generate homozygous clonal tissue (Adler *et al.*, 1998; Strutt and Strutt, 2002; Germani *et al.*, 2018). We compared the microtubule organisation in the control tissue with wild-type *ds* against the mutant clonal tissue, as detected by the presence

or absence of β-galactosidase, respectively (Figure 8A). In *ds* clones in both distal and posterior regions, microtubules remained aligned with each other according to the cell eccentricity (Figure 8B-C), and in both regions the correlations between MTSD and cell eccentricity were unaffected (Figure 8D). Concurrently, clone cells increased their eccentricities in both regions (Figure 8E). Thus, both loss and overexpression of Ds can increase cellular elongation suggesting that it is loss of the polarity rather than the levels of Ft-Ds complexes that contribute to the cell shape phenotype. The microtubule angle in the mutant cells remained coupled with the cell angle, regardless of the region, with the same percentages of angles in 0±45° quadrants (Figure 8F-G).

To summarise, while we found evidence for the Ft-Ds pathway affecting both cell shape and the localisation of the microtubule minus-end capping protein Patronin, these effects do not produce detectable changes in the organisation of the subapical microtubule network. Specifically, they do not influence how well the microtubules align with each other inside cells and the direction in which the overall network orients. Based on our experimental data we concluded that cell shape is the primary cue for the direction and alignment of the subapical microtubule network in *Drosophila* pupal wings.

Discussion

Our work has revealed three key findings. Firstly, we found that the cell shape polarity (the direction in which cells elongate) and Ft-Ds planar polarity are uncoupled in *Drosophila* pupal wings. Secondly, assisted by this uncoupling of two polarities, we demonstrated that subapical microtubule networks orient themselves in agreement with the cell shape rather than planar polarity established by the Ft-Ds complexes. Finally, we found that the Ft-Ds complexes promote the recruitment of the microtubule minus-end capping protein Patronin to cell boundaries, although any contribution of this recruitment to the organisation of subapical microtubule networks in the pupal wing was not detectable.

Cell shape is ultimately determined by a tug-of-war between tissue-scale forces such as shear stress and the forces generated internally within the cell by the cytoskeleton (Mao and Baum, 2015). Ft-Ds planar polarity is established by the developmental programme, namely, by opposing expression gradients of Ds and the Golgi-localised kinase Four-jointed (reviewed in Strutt and Strutt, 2021). In turn, Ft-Ds complexes are reported to actively control cell shape by asymmetrically localising the atypical myosin Dachs, which creates anisotropic junctional tension promoting cellular elongation (Mao *et al.*, 2011; Bosveld *et al.*, 2012). As

a result, the Ft-Ds pathway promotes the alignment of cell angles in such epithelia as the *Drosophila* abdomen (Mangione and Martín-Blanco, 2018). At the same time, cell elongation is also influenced by the axis of mechanical forces in an epithelium – indeed, tissue-scale anisotropic stress applied to epithelial monolayers leads to cellular elongation in the direction of the applied force in both *Drosophila* and vertebrate cells (Aigouy *et al.*, 2010; Wyatt *et al.*, 2015; Duda *et al.*, 2019; Nestor-Bergmann *et al.*, 2019).

Interestingly, we find that depending on the region of the pupal wing, the cell shape and Ft-Ds polarity vectors either align (in the distal region) or not (in the posterior region below vein 4) (Figure 2E-F). We also observed that reduced Ds polarity due to either its loss or overexpression led to an increase in cell elongation (Figures 7C and 8D). Such an uncoupling between cell shape and Ds polarity could be caused by several factors. Firstly, although we did not observe gross differences in the strength of Ds polarity between the two studied regions (Figures 2C), it is possible that due to the presence of additional yet unidentified factors, the degree to which the Ft-Ds complexes activate Dachs differs between the two regions. Note, that as in other tissues, Ft-Ds promote polarised recruitment of Dachs to cell junctions in the pupal wing (Merkel et al., 2014). Lowered activation of orthogonally oriented Dachs in the posterior region would allow the proximodistal global tension to override the Dachs-dependent internal forces and align the cell elongation pattern along the vector of tissue-scale stress. Secondly, dissipation of the external stress that originates from contraction of the wing hinge due to the viscoelastic properties of epithelial cells may lead to a non-uniform distribution of stress in the pupal wing. Indeed, such a non-uniform stress distribution is suggested by the differences in the anisotropy of the response to laser ablation experiments (Etournay *et al.*, 2015). However, the reported anisotropy of the recoil in response to laser cuts was lower in the posterior region than distal (Etournay *et al.*, 2015), which makes it unlikely that the lack of alignment of cell elongation with the Ft-Ds polarity can be solely explained by higher tissue-scale stress in this region. It is also possible that other factors such as the core planar polarity pathway or adherens junctions contribute to determining the cell shape and elongation direction. Such combinatorial regulation of cell shape agrees with the observation that the clones of cells that lack *ft* have either normal or irregular geometries depending on the clone position in pupal wings (Ma *et al.*, 2008). Dissecting the contributions of individual factors and interactions between them would be essential for understanding how cells are shaped in epithelia and how the tissue's ultimate form is established.

11

Regardless of the mechanism that establishes the cell shape polarity, we found that it is this cell shape that the subapical microtubule network follows. Namely, we demonstrated that the overall direction of microtubules follows the cell's long axis whereas the alignment of microtubules with each other is consistent with the cell eccentricity in agreement with the robustness of this alignment previously reported (Płochocka *et al.*, 2021). A similar role for cell shape in organising microtubule polarity independently of Ft-Ds polarity has also been suggested in the *Drosophila* larval epidermis (Pietra *et al.*, 2020).

The instructive role of the cell shape in the organisation of the subapical microtubule network is consistent with the model whereby microtubules 'passively' sense the cell shape constraints due to their dynamic instability (Gomez *et al.*, 2016). Specifically, as the frequency of microtubule catastrophe in the cytoplasm is low *in vivo* (Rogers *et al.*, 2002; Komarova *et al.*, 2009), microtubules grow until they reach the cell boundary, where they either undergo a catastrophe or "zip" with the boundary to continue growing along it depending on the angle of approach (Gomez *et al.*, 2016). In this scenario, any role of the Ft-Ds complexes in the organisation of the subapical microtubule network is indirect through their effects on the cell shape. If by recruiting Dachs and thus, increasing the anisotropy of junctional tension, the Ft-Ds pathway is able to override other cues such as the global tissue stress, the microtubules will follow this new shape aligning according to Ft-Ds localisation – we suggest that such a scenario may be observed in *Drosophila* wing discs (Mao *et al.*, 2011; Matis *et al.*, 2014).

Finally, we found that the Ft-Ds complexes promote the localisation of Patronin as it is enriched within Ds puncta in wings with normal Ft-Ds function and its levels are elevated at cell boundaries following Ds overexpression. This recruitment did not appear to have a detectable effect on the organisation of the subapical microtubule network, which correlated with the cell shape alone in the pupal wing. Previously, it was suggested that the localisation of microtubule minus ends influences how well the microtubules align with each other within a cell (Płochocka *et al.*, 2021). While it does not appear to be the case in pupal wings studied here, it might occur in other tissue contexts where the Ft-Ds complexes exert stronger effects, for example, in *Drosophila* abdomen, where both the Ft-Ds pathway and Patronin have major contributions to shaping the tissue during morphogenesis (Mangione and Martín-Blanco, 2018; Panzade and Matis, 2021).

Altogether, our findings highlight the central role of cell shape/elongation in the organisation of the subapical microtubules. We conclude that while the Ft-Ds pathway is

likely to participate in regulating cell shape, it is not the only contributing factor and can be overridden by other cues. These findings were enabled by our simultaneous analysis on a cell-by-cell basis of three parameters – cell shape, planar cell polarity and microtubule organisation – from microscopy images. The example of planar polarity-microtubule-cell shape relationships studied here shows that such multi-factorial image analyses and integration of relevant parameters aids the dissection of relationships between protein distribution, subcellular organisation and tissue morphogenesis.

Materials and Methods

Key reagents and tool table

Reagent/Resource	Source	ID/Catalog Number
Drosophila strains		
ds-EGFP	(Brittle *et al.*, 2012)	FLYB: FBti0202074
ft-EGFP	(Hale *et al.*, 2015)	
Ubi-p63E-Patronin.A.GFP[3M]	(Wang *et al.*, 2013)	BDSC:55129, FLYB:FBst0055129, RRID:BDSC_55129
P[w+, UAS-FRT-stop-FRT-ds]	This study	
y w hsFLP	Bloomington Drosophila Stock Center (Golic and Lindquist, 1989)	BDSC:7; FLYB:FBti0002044; RRID:BDSC_7
hh-GAL4	(Tanimoto *et al.*, 2000)	FLYB: FBal0121962
ds^{UA071}	(Adler *et al.*, 1998)	BDSC:41784; FLYB:FBal0089339; RRID:BDSC_41784
FRT40	Bloomington Drosophila Stock Center (Xu and Rubin, 1993)	FLYB: FBti0002071

y w P[w+, UbxFLP]1	Bloomington Drosophila Stock Center (Emery *et al.*, 2005)	BDSC:42718; FLYB:FBti0150334; RRID:BDSC_42718
P[w+, arm-lacZ] FRT40	Bloomington Drosophila Stock Center	BDSC:7371; RRID:BDSC_7371
Antibodies		
Mouse monoclonal anti-α-tubulin 1:1000	Sigma-Aldrich	Cat#SC-32293
Mouse monoclonal anti-armadillo 1:100	Developmental Studies Hybridoma Bank	Cat#N2 7A1
Rat monoclonal anti-E-cad 1:200	Developmental Studies Hybridoma Bank	Cat#DCAD2
Rabbit anti-Ds affinity purified 1:50	(Strutt and Strutt, 2002)	N/A
Software		
FV10-ASW	Olympus	N/A
Zen	Zeiss	N/A
Fiji (ImageJ)	https://fiji.sc	N/A
Tissue Analyzer	Benoit Aigouy (Aigouy *et al.*, 2010).	N/A
QuantifyPolarity	Sara Tan (Tan *et al.*, 2021).	N/A
MATLAB R2019b	Mathworks	N/A
GraphPad Prism Version 7	GraphPad Software	N/A
Office Excel 16	Microsoft	N/A
Illustrator 20	Adobe	N/A
Custom scripts for MATLAB	N Bulgakova (https://github.com/nbul)	N/A
Other		
FV1000 confocal microscope	Olympus	N/A

LSM 880 Airyscan Microsope	Zeiss	N/A

Fly genetics and husbandry

Drosophila melanogaster were raised on standard cornmeal/agar/molasses media at 18°C or 25°C unless otherwise specified. Constructs are detailed in the Resource table. To express constructs of interest, the GAL4/UAS system was used (Brand and Perrimon, 1993), with the *hedgehog-GAL4* (*hh-Gal4*) driver. Prepupa individuals were selected and scored against selection markers and aged for 24 hours at 25°C before dissecting.

Induction and recombination experiments

hsFLP was used to excise an FRT-Stop-FRT cassette to allow expression of Ds in the posterior compartment under control of *hh-GAL4* (*hh-GAL4/UAS-FRT-Stop-FRT-ds*). Heat shocks were performed for two hours at 37°C at 18h APF, and pupa were left to age for 6 hours at 25°C before dissecting. *P[w+, UAS-FRT-Stop-FRT-ds]* was generated by cloning the *ds* CDS in the vector pUASt with insertion of a removable stop cassette between the promoter and the CDS, and random integration into the genome by P-element transgenesis. *ds^{UA071}* clones were generated using *UbxFLP* in the X chromosome and FRT40 with *P[w+, arm-lacZ]* FRT40 to mark cells where recombination did not occur.

Dissection and Immunostaining

Pupal wings were dissected as described previously (Strutt, 2001). Pupae without cuticles were fixed with paraformaldehyde in PBS (PP) and wings dissected away, with 10% PP for a total of 60 minutes in assays involving microtubule imaging and 4% PP for 40 minutes for all other labelling. Pupal wings were blocked for 60 minutes in PBS containing 0.3% Triton X-100 (PBST) and 10% normal goat serum (NGS). Wings were incubated with primary antibodies and 10% NGS PBST overnight at 4°C, washed ten times in PBST, incubated overnight with secondary antibodies and 10% NGS PBST overnight at 4°C, and washed in PBST again. Antibodies are listed in the Reagents and Tools table. Finally, wings were equilibrated in Vectashield (Vector Labs, H-1000) and mounted in the same media.

Microscopy

Images were acquired at RT (20-22°C). The sub-apical domain of the cell was identified using the localisation of both tubulin and E-cadherin (see Figure 3). Pupal wings were oriented along the proximodistal axis using v4 as a reference. For analysis of Ds-EGFP and Patronin-GFP distribution and polarity, an upright confocal microscope (FV1000; Olympus) using 60x 1.42 NA oil PlanApoN objective lens was used. 16-bit depth images were taken at a magnification of 12.8 px/µm with 0.15 (Ds-EGFP) or 0.38 (Pat-GFP) µm between z-sections. Images of the subapical microtubule network were acquired using a Zeiss AiryScan microscope and the 63x objective lens. Z-stacks consisted of seven sections with 23.5 px/µm in XY resolution and 0.185 µm distance between sequential Z-sections. All processing was done at 6.5 power in the ZEN software. Representative images used for Figure preparation are the average projections of the region of interest/analysis. Figures were assembled using Adobe CS3 Photoshop and Illustrator (http://www.adobe.com). The processing of images shown in the figures involved adjusting gamma settings.

Image processing

The QuantifyPolarity graphic user interface has been previously described (Tan *et al.*, 2021) and our custom automated image analysis scripts were written for MATLAB and can be found at www.github.com/nbul.

Planar polarity (QuantifyPolarity)

To measure polarity, wing images were aligned along the proximodistal wing axis based on wing vein orientation, and border masks were generated using Tissue Analyzer (Aigouy *et al.*, 2010). On a cell-by-cell basis, the polarity magnitude of membrane proteins was computed using Principle Component Analysis (PCA) in QuantifyPolarity (Tan *et al.*, 2021). In this algorithm, a cell is first transformed onto a regular shape depending on the number of cell vertices. Then, intensities of individual pixels are normalised and the polarity angle is calculated as the angle that produces the largest variance of normalised intensities. Finally, the normalised intensities are converted into pseudo-*XY*-coordinates and the eigenvalues of the covariation matrix of these transformed coordinates are used to compute the polarity magnitude. Importantly, this approach produces cell shape-independent measures of polarity angle and magnitude. The full description of the algorithm and the instructions for downloading are available in (Tan *et al.*, 2021). The same methodology was applied to measure the PCA component of Patronin-GFP and the distributions of E-cadherin and Ds as

16

revealed by immunolabelling. Polarity angles were extracted and drawn over the segmentation masks using our custom automated script in MATLAB (https://github.com/nbul/Cytoskeleton/tree/master/PCP-MT).

Apicobasal intensity

Only the pupal wing regions with cells in the same z-plane across the entire field were used for imaging. Average intensity was measured in each z-section for both Ds-EGFP and tubulin signals. Each z-section measurement was normalised to the maximum average intensity for this protein in every Z-stack, and the different samples were vertically aligned with respect to the maximum tubulin signal distribution. Average intensity profiles across all the samples were then calculated for both Ds-EGFP and tubulin signals.

Proximity analysis

The MATLAB script (https://github.com/nbul/Proximity) was used to quantify the spatial proximity between tubulin or Patronin-GFP signals and the Ds puncta. The masks generated using Tissue Analyzer (Aigouy *et al.*, 2010) were cleared of any cells contacting image borders and dilated using a disc-shaped structuring element with a radius of 3 px. The average signal intensities within cells defined by these dilated masks were used to calculate the cytoplasm intensity from average intensity projections of Z-stacks with tubulin, Patronin-GFP or Ds signals. These average intensity projections were adjusted so that 0.5% of the pixels with the lowest intensities were set to black and the 0.5% of the pixels with the highest intensities were set to white to normalise the variability in signal between images and datasets but maintain the relative differences between different regions within each image. Then, Ds puncta were defined by thresholding images with the average projection of the Ds signal using a global threshold calculated using Otsu's method and multiplied by an empirically determined factor (=2.5). The overlap between the dilated masks and thresholded Ds puncta was used to determine the puncta and non-puncta boundary regions and calculate their respective average intensities. Images with isolated puncta and non-puncta regions were then dilated using a disc-shaped structuring element with a radius of 8 px. Following subtraction of undilated puncta and non-puncta regions, these images were used to calculate the average intensities of puncta and non-puncta halos (areas directly adjacent to cell boundaries regions with Ds puncta or depleted of Ds).

Microtubules

For the analysis of the subapical microtubule network, we employed a protocol previously developed by us (Gomez *et al.*, 2016; Płochocka *et al.*, 2021). The average projections of

17

images with tubulin signals were adjusted so that 0.5% of the pixels with the lowest intensities were set to black and the 0.5% of the pixels with the highest intensities were set to white to normalise the variability in signal between images and increase the contrast. Masks generated using Tissue Analyzer (Aigouy *et al.*, 2010) were used to isolate tubulin signals in individual cells. Then, the magnitude of the tubulin signal according to its direction (gradient of the signal) in each cell was calculated by convolving the tubulin signal using two 5×5 Sobel operators (Gomez *et al.*, 2016). The resulting distributions of tubulin signals were aligned to their maxima at 0 and averaged for cells with specified eccentricities (0.750 ± 0.025 and 0.800 ± 0.025) to produce average profiles of microtubule angle distributions in cells (as in Figure 5) (Płochocka *et al.*, 2021). At the same time, the unaltered distributions were fitted with the Von Mises distribution and the estimated mean and standard deviation of the fitted curve in each cell. The mean was used as the main direction of the subapical microtubule network in this cell and the standard deviation as the measure of the microtubule alignment with each other (Microtubule Standard Deviation, MTSD). Finally, the cell directions were calculated by fitting the pixel coordinates of each cell isolated using masks to an ellipse and obtaining the direction of the long axis of the best-fit ellipse. MTSD was plotted against cell eccentricity for cells with a MTSD <90 excluding cells with unfittable distributions of tubulin signal. The discarded cells (cells/% of total) were: Figure 5C 8/7% (distal) and 5/2% (posterior); Figure 7C 16/4% (*distal control*), 9/3% (*distal Ds OE*), 11/3% (*posterior control*) and 9/2% (*posterior Ds OE*); Figure 8D 11/8% (*distal control*), 7/4% (*distal ds*), 4/2% (*posterior control*) and 2/1% (*posterior ds*). The MATLAB code used in this study is available at https://github.com/nbul/Cytoskeleton/tree/master/PCP-MT.

Angle visualisation and quantification

Data about directions of cell elongation (the direction of the long axis of the best-fit ellipse), overall directions of microtubule networks and Ds polarity angle (transferred from QuantifyPolarity) were plotted on image masks produced using Tissue Analyzer (Aigouy *et al.*, 2010). The length of plotted lines does not reflect polarity magnitudes or length of elongation but is fixed at half of the average long cell axis. Average cell orientation within each biological replicate/image was used to normalise the Ds polarity angle, individual cell orientations and microtubule angles for each cell in polar histograms with 9 bins in 0-180° format. Data were mirrored to ease visualisation. Normalised angle data was also used to separate angles into quadrants: 0±45° and 90±45°. The plotting and calculations were

performed within the script for the microtubule organisation analysis (https://github.com/nbul/Cytoskeleton/tree/master/PCP-MT).

Statistical Analysis

Datasets were subjected to D'Agostino & Pearson test to determine normality (Shapiro-Wilk test was used for small datasets). PCA polarity magnitude, average intensity in different regions were tested with One-Way ANOVA (normal distribution) or Friedman test (non-normal distribution), with multiple comparisons performed with Tukey's or Dunn's tests, respectively. Datasets in different regions were paired when belonging to the same biological replicate (individual). The curve fitting of cell eccentricities was compared with Extra sum-of-squares F test. Average border intensity of Pat-GFP was compared with Brown-Forsythe and Welch ANOVA test and Dunnett's T3 test for multiple comparisons (comparisons with *Ds OE*) or paired t-test (regions from the control genotype). The relationships between MTSD and cell eccentricity were tested between regions or genotypes by comparing their respective Pearson's correlations using the bootstrap method (Wilcox, 2009). Percentage of angles in the proximodistal quadrant (0±45°) for PCP polarity, average microtubule orientation or cell angle were compared using either: One-Way ANOVA (normal distribution, Figure 2), Kruskal-Wallis (non-normal distribution) or Two-Way ANOVA (polarity data in Figure 6). Multiple comparisons were performed with Brown-Forsythe and Welch (for ANOVAs), Dunn's (for Kruskal-Wallis) or Šidák tests.

Data availability

The generated *Drosophila* strains are available upon request. All in-house scripts are available at https://github.com/nbul/.

Acknowledgements

Competing Interests

The authors declare no competing interests.

Author Contribution

N.A.B. and D.S. devised the project. N.A.B., D.S. and M.R.M. designed the experimental plan. M.R.M. and R.H. conducted the experiments. M.R.M. and N.A.B. analysed the data. M.R.M., N.A.B. and D.S. wrote the manuscript.

Acknowledgements

References

Adler, P.N., Charlton, J., and Liu, J. (1998). Mutations in the cadherin superfamily member gene dachsous cause a tissue polarity phenotype by altering frizzled signaling. Development *125*, 959-968.

Aigouy, B., Farhadifar, R., Staple, D.B., Sagner, A., Röper, J.C., Jülicher, F., and Eaton, S. (2010). Cell flow reorients the axis of planar polarity in the wing epithelium of Drosophila. Cell *142*, 773-786.

Akhmanova, A., and Kapitein, L.C. (2022). Mechanisms of microtubule organization in differentiated animal cells. Nat Rev Mol Cell Biol *23*, 541-558.

Bosveld, F., Bonnet, I., Guirao, B., Tlili, S., Wang, Z., Petitalot, A., Marchand, R., Bardet, P.L., Marcq, P., Graner, F., and Bellaïche, Y. (2012). Mechanical control of morphogenesis by Fat/Dachsous/Four-jointed planar cell polarity pathway. Science *336*, 724-727.

Brand, A.H., and Perrimon, N. (1993). Targeted gene expression as a means of altering cell fates and generating dominant phenotypes. Development *118*, 401-415.

Brittle, A., Thomas, C., and Strutt, D. (2012). Planar polarity specification through asymmetric subcellular localization of Fat and Dachsous. Curr Biol *22*, 907-914.

Bulgakova, N.A., Grigoriev, I., Yap, A.S., Akhmanova, A., and Brown, N.H. (2013). Dynamic microtubules produce an asymmetric E-cadherin-Bazooka complex to maintain segment boundaries. J Cell Biol *201*, 887-901.

Butler, M.T., and Wallingford, J.B. (2017). Planar cell polarity in development and disease. Nat Rev Mol Cell Biol *18*, 375-388.

Chien, Y.H., Keller, R., Kintner, C., and Shook, D.R. (2015). Mechanical strain determines the axis of planar polarity in ciliated epithelia. Curr Biol *25*, 2774-2784.

Devenport, D. (2014). The cell biology of planar cell polarity. J Cell Biol *207*, 171-179.

Duda, M., Kirkland, N.J., Khalilgharibi, N., Tozluoglu, M., Yuen, A.C., Carpi, N., Bove, A., Piel, M., Charras, G., Baum, B., and Mao, Y. (2019). Polarization of Myosin II Refines Tissue Material Properties to Buffer Mechanical Stress. Dev Cell *48*, 245-260.e247.

Emery, G., Hutterer, A., Berdnik, D., Mayer, B., Wirtz-Peitz, F., Gaitan, M.G., and Knoblich, J.A. (2005). Asymmetric Rab 11 endosomes regulate delta recycling and specify cell fate in the Drosophila nervous system. Cell *122*, 763-773.

Etournay, R., Popović, M., Merkel, M., Nandi, A., Blasse, C., Aigouy, B., Brandl, H., Myers, G., Salbreux, G., Jülicher, F., and Eaton, S. (2015). Interplay of cell dynamics and epithelial tension during morphogenesis of the Drosophila pupal wing. Elife *4*, e07090.

Germani, F., Bergantinos, C., and Johnston, L.A. (2018). Mosaic Analysis in Drosophila. Genetics *208*, 473-490.

Golic, K.G., and Lindquist, S. (1989). The FLP recombinase of yeast catalyzes site-specific recombination in the Drosophila genome. Cell *59*, 499-509.

21

Gomez, J.M., Chumakova, L., Bulgakova, N.A., and Brown, N.H. (2016). Microtubule organization is determined by the shape of epithelial cells. Nat Commun *7*, 13172.

Goodrich, L.V., and Strutt, D. (2011). Principles of planar polarity in animal development. Development *138*, 1877-1892.

Goodwin, S.S., and Vale, R.D. (2010). Patronin regulates the microtubule network by protecting microtubule minus ends. Cell *143*, 263-274.

Hale, R., Brittle, A.L., Fisher, K.H., Monk, N.A., and Strutt, D. (2015). Cellular interpretation of the long-range gradient of Four-jointed activity in the Drosophila wing. Elife *4*, e05789.

Harumoto, T., Ito, M., Shimada, Y., Kobayashi, T.J., Ueda, H.R., Lu, B., and Uemura, T. (2010). Atypical cadherins Dachsous and Fat control dynamics of noncentrosomal microtubules in planar cell polarity. Dev Cell *19*, 389-401.

Herawati, E., Taniguchi, D., Kanoh, H., Tateishi, K., Ishihara, S., and Tsukita, S. (2016). Multiciliated cell basal bodies align in stereotypical patterns coordinated by the apical cytoskeleton. J Cell Biol *214*, 571-586.

Hirano, S., Mii, Y., Charras, G., and Michiue, T. (2022). Alignment of cell long axis by unidirectional tension acts cooperatively with Wnt signalling to establish PCP. Development *149*, dev200515.

Hirokawa, N., and Takemura, R. (2005). Molecular motors and mechanisms of directional transport in neurons. Nat Rev Neurosci *6*, 201-214.

Kimura, T., Saito, H., Kawasaki, M., and Takeichi, M. (2021). CAMSAP3 is required for mTORC1-dependent ependymal cell growth and lateral ventricle shaping in mouse brains. Development *148*, dev195073.

Komarova, Y., De Groot, C.O., Grigoriev, I., Gouveia, S.M., Munteanu, E.L., Schober, J.M., Honnappa, S., Buey, R.M., Hoogenraad, C.C., Dogterom, M., Borisy, G.G., Steinmetz, M.O., and Akhmanova, A. (2009). Mammalian end binding proteins control persistent microtubule growth. J Cell Biol *184*, 691-706.

Lawrence, P.A., and Casal, J. (2018). Planar cell polarity: two genetic systems use one mechanism to read gradients. Development *145*, dev168229.

Li-Villarreal, N., Forbes, M.M., Loza, A.J., Chen, J., Ma, T., Helde, K., Moens, C.B., Shin, J., Sawada, A., Hindes, A.E., Dubrulle, J., Schier, A.F., Longmore, G.D., Marlow, F.L., and Solnica-Krezel, L. (2015). Dachsous1b cadherin regulates actin and microtubule cytoskeleton during early zebrafish embryogenesis. Development *142*, 2704-2718.

Ma, D., Amonlirdviman, K., Raffard, R.L., Abate, A., Tomlin, C.J., and Axelrod, J.D. (2008). Cell packing influences planar cell polarity signaling. Proc Natl Acad Sci U S A *105*, 18800-18805.

Ma, D., Yang, C.H., McNeill, H., Simon, M.A., and Axelrod, J.D. (2003). Fidelity in planar cell polarity signalling. Nature *421*, 543-547.

Mangione, F., and Martín-Blanco, E. (2018). The Dachsous/Fat/Four-Jointed Pathway Directs the Uniform Axial Orientation of Epithelial Cells in the Drosophila Abdomen. Cell Rep *25*, 2836-2850.

Mao, Y., and Baum, B. (2015). Tug of war--the influence of opposing physical forces on epithelial cell morphology. Dev Biol *401*, 92-102.

Mao, Y., Tournier, A.L., Bates, P.A., Gale, J.E., Tapon, N., and Thompson, B.J. (2011). Planar polarization of the atypical myosin Dachs orients cell divisions in Drosophila. Genes Dev *25*, 131-136.

Masucci, E.M., Relich, P.K., Lakadamyali, M., Ostap, E.M., and Holzbaur, E.L.F. (2022). Microtubule dynamics influence the retrograde biased motility of kinesin-4 motor teams in neuronal dendrites. Mol Biol Cell *33*, mbcE21100480.

Matis, M., Russler-Germain, D.A., Hu, Q., Tomlin, C.J., and Axelrod, J.D. (2014). Microtubules provide directional information for core PCP function. Elife *3*, e02893.

Merkel, M., Sagner, A., Gruber, F.S., Etournay, R., Blasse, C., Myers, E., Eaton, S., and Jülicher, F. (2014). The balance of prickle/spiny-legs isoforms controls the amount of coupling between core and fat PCP systems. Curr Biol *24*, 2111-2123.

Nestor-Bergmann, A., Stooke-Vaughan, G.A., Goddard, G.K., Starborg, T., Jensen, O.E., and Woolner, S. (2019). Decoupling the Roles of Cell Shape and Mechanical Stress in Orienting and Cueing Epithelial Mitosis. Cell Rep *26*, 2088-2100.

Olofsson, J., Sharp, K.A., Matis, M., Cho, B., and Axelrod, J.D. (2014). Prickle/spiny-legs isoforms control the polarity of the apical microtubule network in planar cell polarity. Development *141*, 2866-2874.

Panzade, S., and Matis, M. (2021). The Microtubule Minus-End Binding Protein Patronin Is Required for the Epithelial Remodeling in the Drosophila Abdomen. Front Cell Dev Biol *9*, 682083.

Pietra, S., Ng, K., Lawrence, P.A., and Casal, J. (2020). Planar cell polarity in the larval epidermis of Drosophila and the role of microtubules. Open Biol *10*, 200290.

Płochocka, A.Z., Ramirez Moreno, M., Davie, A.M., Bulgakova, N.A., and Chumakova, L. (2021). Robustness of the microtubule network self-organization in epithelia. Elife *10*, e59529.

Rogers, S.L., Rogers, G.C., Sharp, D.J., and Vale, R.D. (2002). Drosophila EB1 is important for proper assembly, dynamics, and positioning of the mitotic spindle. J Cell Biol *158*, 873-884.

Sepich, D.S., Usmani, M., Pawlicki, S., and Solnica-Krezel, L. (2011). Wnt/PCP signaling controls intracellular position of MTOCs during gastrulation convergence and extension movements. Development *138*, 543-552.

Shimada, Y., Yonemura, S., Ohkura, H., Strutt, D., and Uemura, T. (2006). Polarized transport of Frizzled along the planar microtubule arrays in Drosophila wing epithelium. Dev Cell *10*, 209-222.

Siegrist, S.E., and Doe, C.Q. (2007). Microtubule-induced cortical cell polarity. Genes Dev *21*, 483-496.

Silva, E., Tsatskis, Y., Gardano, L., Tapon, N., and McNeill, H. (2006). The tumor-suppressor gene fat controls tissue growth upstream of expanded in the hippo signaling pathway. Curr Biol *16*, 2081-2089.

Singh, A., Saha, T., Begemann, I., Ricker, A., Nüsse, H., Thorn-Seshold, O., Klingauf, J., Galic, M., and Matis, M. (2018). Polarized microtubule dynamics directs cell mechanics and coordinates forces during epithelial morphogenesis. Nat Cell Biol *20*, 1126-1133.

Steinhauer, J., and Kalderon, D. (2006). Microtubule polarity and axis formation in the Drosophila oocyte. Developmental Dynamics *235*, 1455-1468.

Strutt, D.I. (2001). Asymmetric localization of frizzled and the establishment of cell polarity in the Drosophila wing. Mol Cell *7*, 367-375.

Strutt, H., and Strutt, D. (2002). Nonautonomous planar polarity patterning in Drosophila: dishevelled-independent functions of frizzled. Dev Cell *3*, 851-863.

Strutt, H., and Strutt, D. (2021). How do the Fat-Dachsous and core planar polarity pathways act together and independently to coordinate polarized cell behaviours? Open Biol *11*, 200356.

Tan, S.E., Tan, W., Fisher, K.H., and Strutt, D. (2021). QuantifyPolarity, a new tool-kit for measuring planar polarized protein distributions and cell properties in developing tissues. Development *148*, dev198952.

Tanimoto, H., Itoh, S., ten Dijke, P., and Tabata, T. (2000). Hedgehog creates a gradient of DPP activity in Drosophila wing imaginal discs. Mol Cell *5*, 59-71.

Tateishi, K., Nishida, T., Inoue, K., and Tsukita, S. (2017). Three-dimensional Organization of Layered Apical Cytoskeletal Networks Associated with Mouse Airway Tissue Development. Sci Rep *7*, 43783.

Toya, M., and Takeichi, M. (2016). Organization of Non-centrosomal Microtubules in Epithelial Cells. Cell Struct Funct *41*, 127-135.

van Haren, J., and Wittmann, T. (2019). Microtubule Plus End Dynamics - Do We Know How Microtubules Grow?: Cells boost microtubule growth by promoting distinct structural transitions at growing microtubule ends. Bioessays *41*, e1800194.

Vladar, E.K., Bayly, R.D., Sangoram, A.M., Scott, M.P., and Axelrod, J.D. (2012). Microtubules enable the planar cell polarity of airway cilia. Curr Biol *22*, 2203-2212.

Vu, H.T., Mansour, S., Kücken, M., Blasse, C., Basquin, C., Azimzadeh, J., Myers, E.W., Brusch, L., and Rink, J.C. (2019). Dynamic Polarization of the Multiciliated Planarian Epidermis between Body Plan Landmarks. Dev Cell *51*, 526-542.e526.

Wang, H., Brust-Mascher, I., Civelekoglu-Scholey, G., and Scholey, J.M. (2013). Patronin mediates a switch from kinesin-13-dependent poleward flux to anaphase B spindle elongation. J Cell Biol *203*, 35-46.

Wilcox, R.R. (2009). Comparing Pearson Correlations: Dealing with Heteroscedasticity and Nonnormality. Communications in Statistics - Simulation and Computation *38*, 2220-2234.

Wu, X., and Hammer, J.A. (2021). ZEISS Airyscan: Optimizing Usage for Fast, Gentle, Super-Resolution Imaging. Methods Mol Biol *2304*, 111-130.

Wyatt, T.P., Harris, A.R., Lam, M., Cheng, Q., Bellis, J., Dimitracopoulos, A., Kabla, A.J., Charras, G.T., and Baum, B. (2015). Emergence of homeostatic epithelial packing and stress dissipation through divisions oriented along the long cell axis. Proc Natl Acad Sci U S A *112*, 5726-5731.

Xu, T., and Rubin, G.M. (1993). Analysis of genetic mosaics in developing and adult Drosophila tissues. Development *117*, 1223-1237.

Zakaria, S., Mao, Y., Kuta, A., de Sousa, C.F., Gaufo, G.O., McNeill, H., Hindges, R., Guthrie, S., Irvine, K.D., and Francis-West, P.H. (2014). Regulation of neuronal migration by Dchs1-Fat4 planar cell polarity. Curr Biol *24*, 1620-1627.

Zhelezov, G., Alfred, V., Bulgakova, N.A., and Chumakova, L. (2019). The walkoff effect: cargo distribution implies motor type in bidirectional microtubule bundles. bioRxiv, 831024.
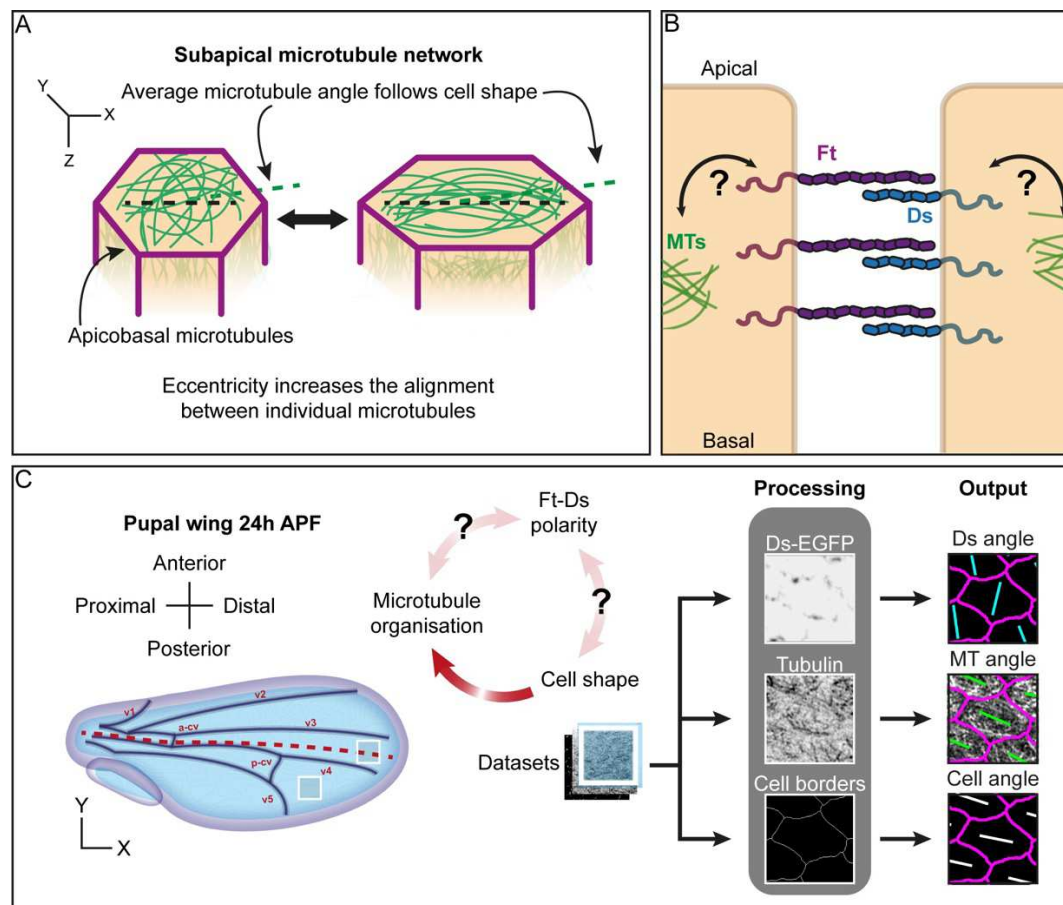
Figures and legends

Figure 1. Development of a toolkit to investigate the effects of cell shape and Ft-Ds polarity on the organisation of the subapical microtubule network.

(A) Cartoon depicting the subapical microtubule network in cells with different elongations.

(B) Cartoon of the planar polarised localisation of the Fat-Dachsous (Ft-Ds) atypical cadherins at the subapical cell-cell boundary and their possible interaction with the subapical microtubule network.

(C) Diagram of a pupal wing at 24h APF with the two regions of interest (distal and posterior) highlighted by white squares and the image analysis pipeline. The main longitudinal veins of the wing (v1-5), and the anterior (a-cv) and posterior (p-cv) crossveins are depicted in black. The combination of software and automated analysis scripts allowed us to extract cell-by-cell data about cell shape (using cell borders) and correlate it with the distribution of proteins at the junctions (e.g. detected with the knock-in Ds-EGFP) and the organisation of the subapical microtubule network (detected by immunolabelling against tubulin).
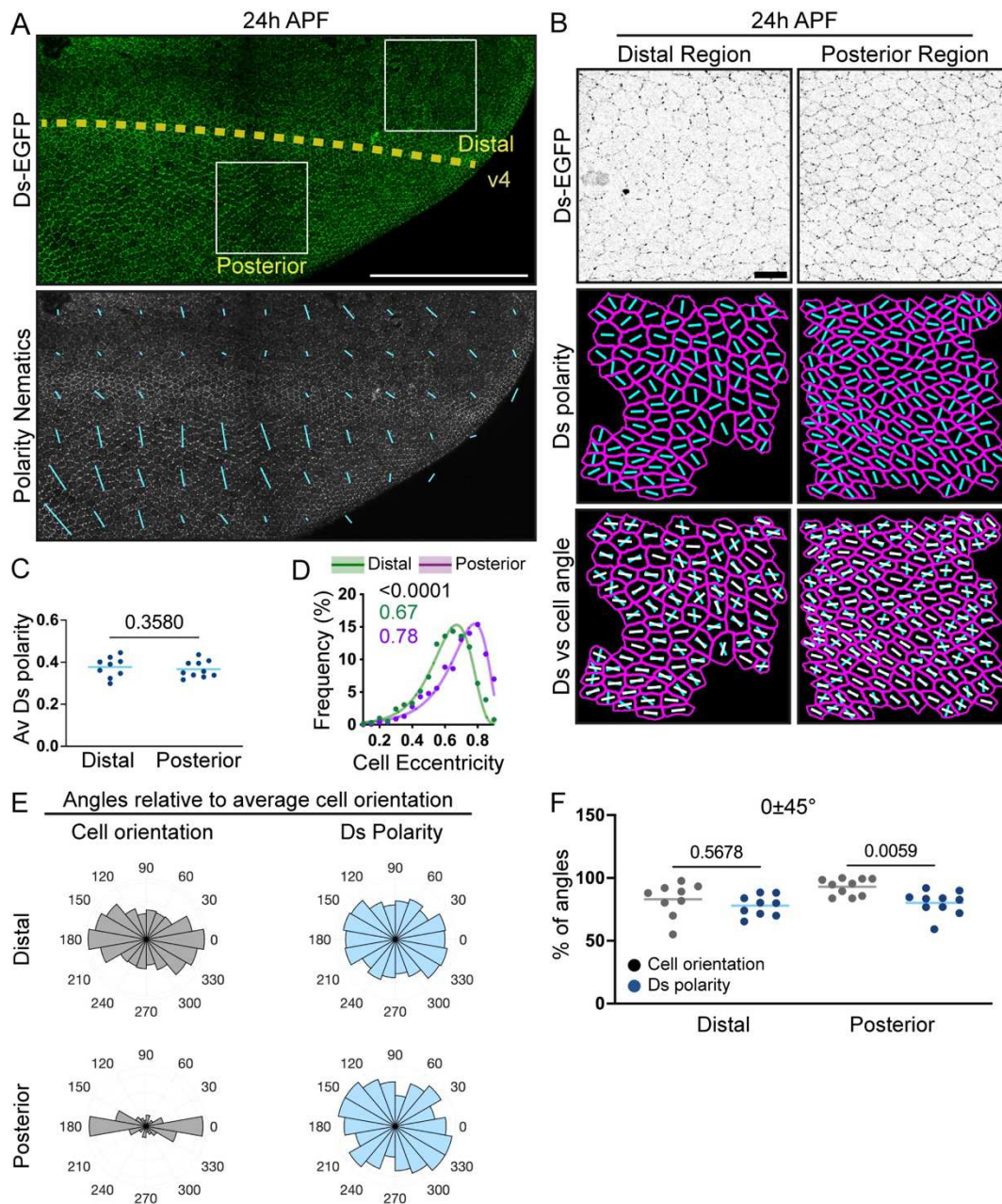
26

Figure 2. Ds exhibits radial/anteroposterior polarity in the wing independently of cell shape at 24h APF.

(A) Apical view of the distoposterior region of a pupal wing at 24h APF expressing Ds-EGFP (green with enhanced brightness, top; greyscale, bottom) and showing the coarse grain polarity nematics (6x6 cells) of Ds-EGFP (blue lines, bottom). The white dotted line indicates the position of longitudinal vein 4 (v4). Scale bar: 100 μm. Distal is to the right and anterior is up in this and all subsequent images (see Figure 1C).

(B) Apical view of cells expressing Ds-EGFP at 24h APF, located at the distal (left) and posterior (right) regions of the pupal wing. Ds-EGFP distribution (inverted greyscale, top),

Ds-EGFP polarity nematics alone (blue lines, middle, cell outlines in magenta) or with cell angle (white lines, bottom) are shown. Scale bar: 10 µm.

(C) Average Ds-EGFP polarity (PCA method) in the two analysed regions. Two-tailed paired t-test (for paired regions in 9 wings). Total data set N=9 (distal) and 10 (posterior) wings.

(D) Distributions of cell eccentricities in the two regions of interest with the binned data points (dots), the best-fit lognormal distributions (lines), the p-value for the probability of the distributions being the same (extra-sum-of-squares F test, black text) and modes of the best-fit distributions (green and magenta text). N= 9 distal and 10 posterior regions.

(E) Polar histograms depicting binned cell orientations (grey) and Ds polarity (blue) relative to the average cell orientation in each region in distal (top) and posterior (bottom) regions of pupal wings at 24h APF. N= cells from 9 distal and 10 posterior regions.

(F) Percentage of individual cell angles per wing region in the 0±45° range relative to the average cell orientation for cell orientation and Ds polarity. Lines represent the mean values. Brown-Forsythe and Welch ANOVA. N= 9 distal and 10 posterior regions.
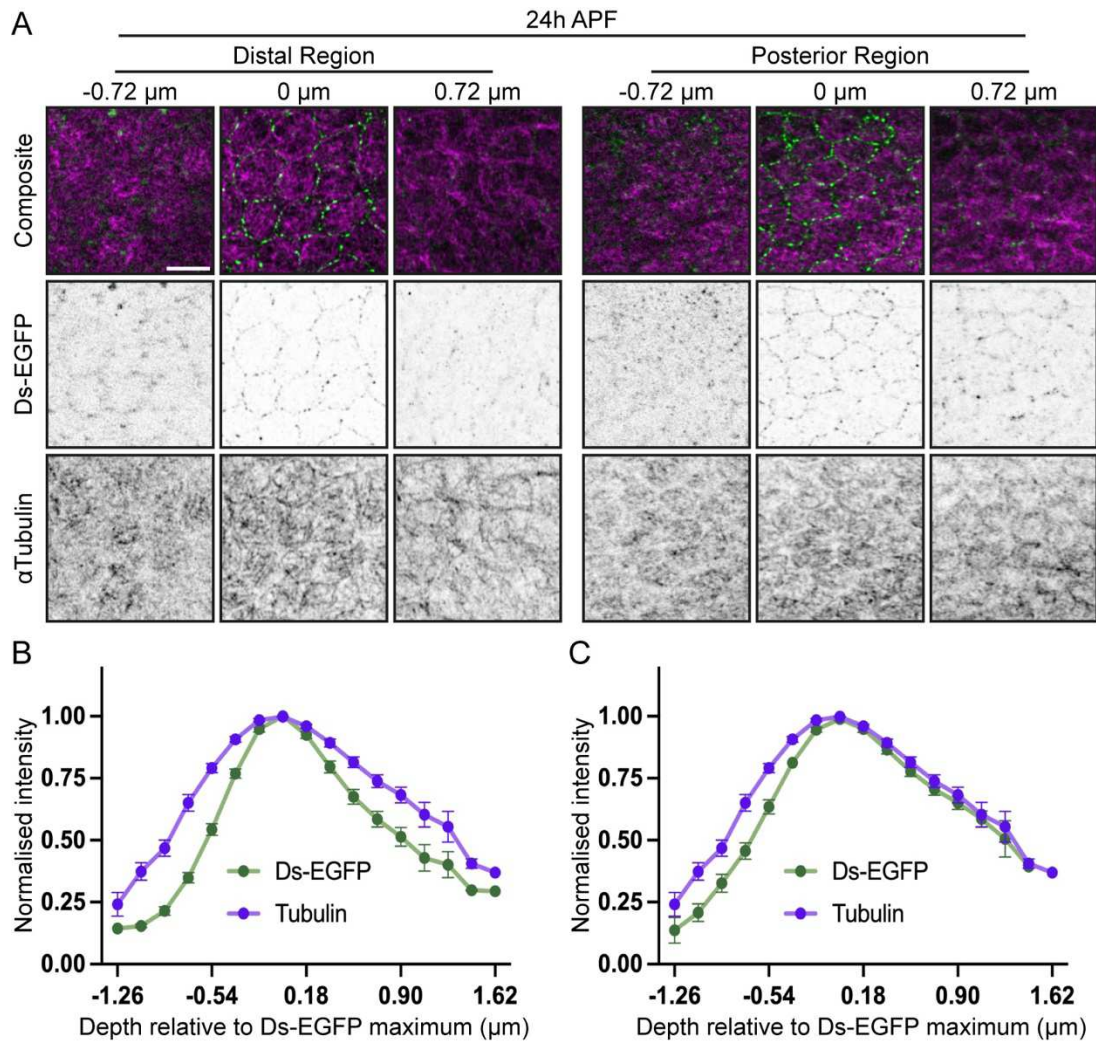
Figure 3. Ft-Ds polarity complexes and the subapical microtubule networks are localised in the same apicobasal position in cells of 24h pupal wings.

(A) Subapical localisation of Ds-EGFP (green, composite top; inverted greyscale, middle panels) and microtubules stained with antibody against tubulin (magenta, top panels; inverted greyscale, bottom panels) at both the distal (left) and posterior (right) regions of the pupal wing 24h APF. Images depict the distribution of both markers at different positions across the apicobasal axis relative to the maximum mean intensity of Ds-EGFP (0 µm). Scale bar: 5 µm.

(B, C) Normalised intensity of Ds-EGFP and tubulin (mean ± s.e.m.) at the distal (B) and posterior (C) regions along the subapical axis, centred around the maximum mean intensity of Ds-EGFP (0 µm). N= 11 wings.
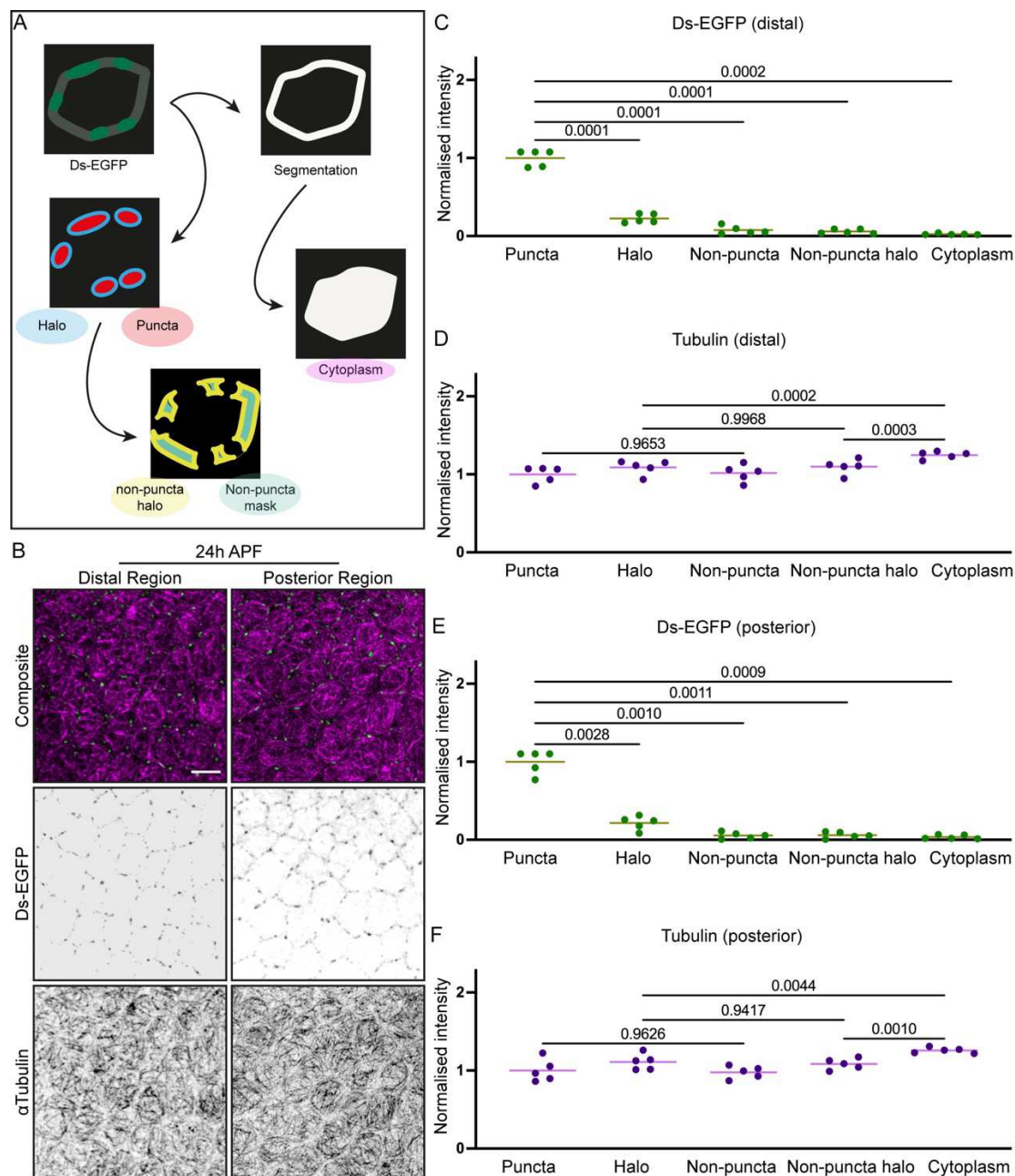
Figure 4. Ft-Ds localisation does not correlate with local changes in the density of apical microtubules at 24h APF.

(A) Cartoon illustrating the analysis pipeline for determining the relative signal levels in different subcellular localisations. The automated script thresholds the images to detect Ds puncta, and thus, classify cell boundary pixels from the dilated segmentation masks into puncta and non-puncta regions. The pixels around the puncta and non-puncta regions (halos) are used to examine local tubulin density in the proximity of the Ds puncta. The average signal inside the cell is used as the cytoplasm intensity.

(B) Apical view of pupal wings at 24h APF expressing Ds-EGFP (green, top; inverted greyscale, middle) and stained against tubulin (magenta, top; inverted greyscale, bottom) corresponding to the distal (left) and posterior (right) regions. Scale bar: 5 µm.

(C-F) Normalised intensity levels of Ds-EGFP (C, E) and tubulin (D, F) at the distal (C, D) and posterior (E, F) regions of the pupal wing, within specific areas as detected by the analysis. Lines represent the mean values. One-way ANOVA with Tukey's multiple comparisons test. N= 5 wings.
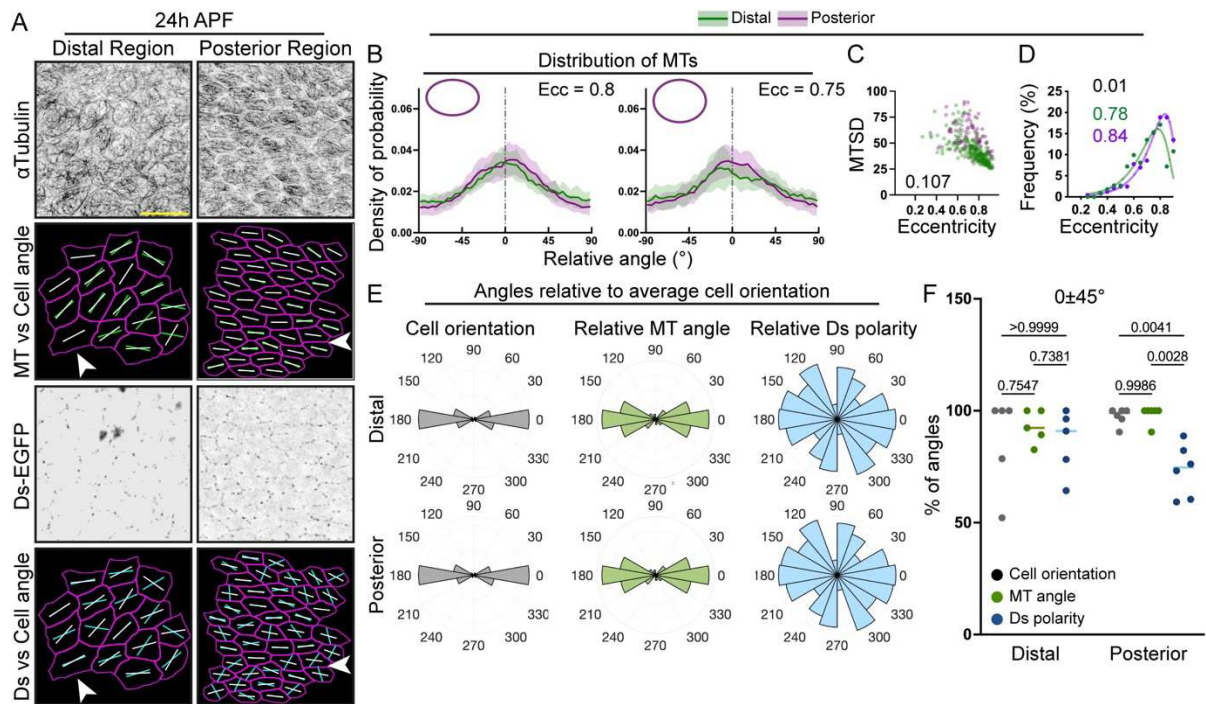
Figure 5. The organisation of subapical microtubule networks in cells with normal expression of Ft-Ds in the pupal wing at 24h APF.

(A) Apical view of cells stained against tubulin (inverted greyscale, top) and expressing Ds-EGFP (inverted greyscale, third row) in the distal (left) and posterior (right) regions of the pupal wing at 24h APF. Microtubule angles (green lines, second row), cell angles (white lines, second and bottom row), and Ds polarities (blue lines, bottom row) in individual cells are shown. White arrowheads indicate examples of cells where Ds polarity is parallel to average microtubule and cell angles (left) or perpendicular (right). Scale bar: 5 μm.

(B) Microtubule angle distributions (line indicates mean, shading indicates standard deviation) relative to the maximum of the tubulin signal in each cell (0°) binned by cell eccentricity (0.8 ± 0.025, left; 0.75 ± 0.025, right) in the distal (green) and posterior (magenta) regions. N= 14 (0.8, distal), 12 (0.75, distal), 44 (0.8, posterior) and 33 (0.75, posterior) cells (5 distal and 6 posterior wings).

(C) Correlation between cell eccentricities and Microtubule Standard Deviation (MTSD) in the distal (green) and posterior (magenta) regions of pupal wings 24h APF. Each dot represents an individual cell, the number indicates the p-value for the Pearson's correlations between the two regions tested being different using the bootstrap method. N= 5 distal and 6 posterior regions.

(D) Distributions of cell eccentricities in the distal (green) and posterior (magenta) regions of pupal wings 24h APF with the binned data points (dots), the best-fit lognormal distributions (lines), the p-value for the probability of the distributions being the same (extra-sum-of-squares F test, black text) and modes of the best-fit distributions (green and magenta text). N= 5 distal and 6 posterior regions.

(E) Polar histograms depicting binned cell orientations (grey), microtubule angles (green) and Ds polarity (blue) relative to the average cell orientation in each region in distal (top) and posterior (bottom) regions of pupal wings at 24h APF. N= 5 distal and 6 posterior regions.

(F) Percentage of individual cell angles in the 0±45° range relative to the average cell orientation for cell orientation, microtubule angle and Ds polarity. Lines represent the mean values. Kruskal-Wallis with Dunn's multiple comparisons test. N= 5 distal and 6 posterior regions.
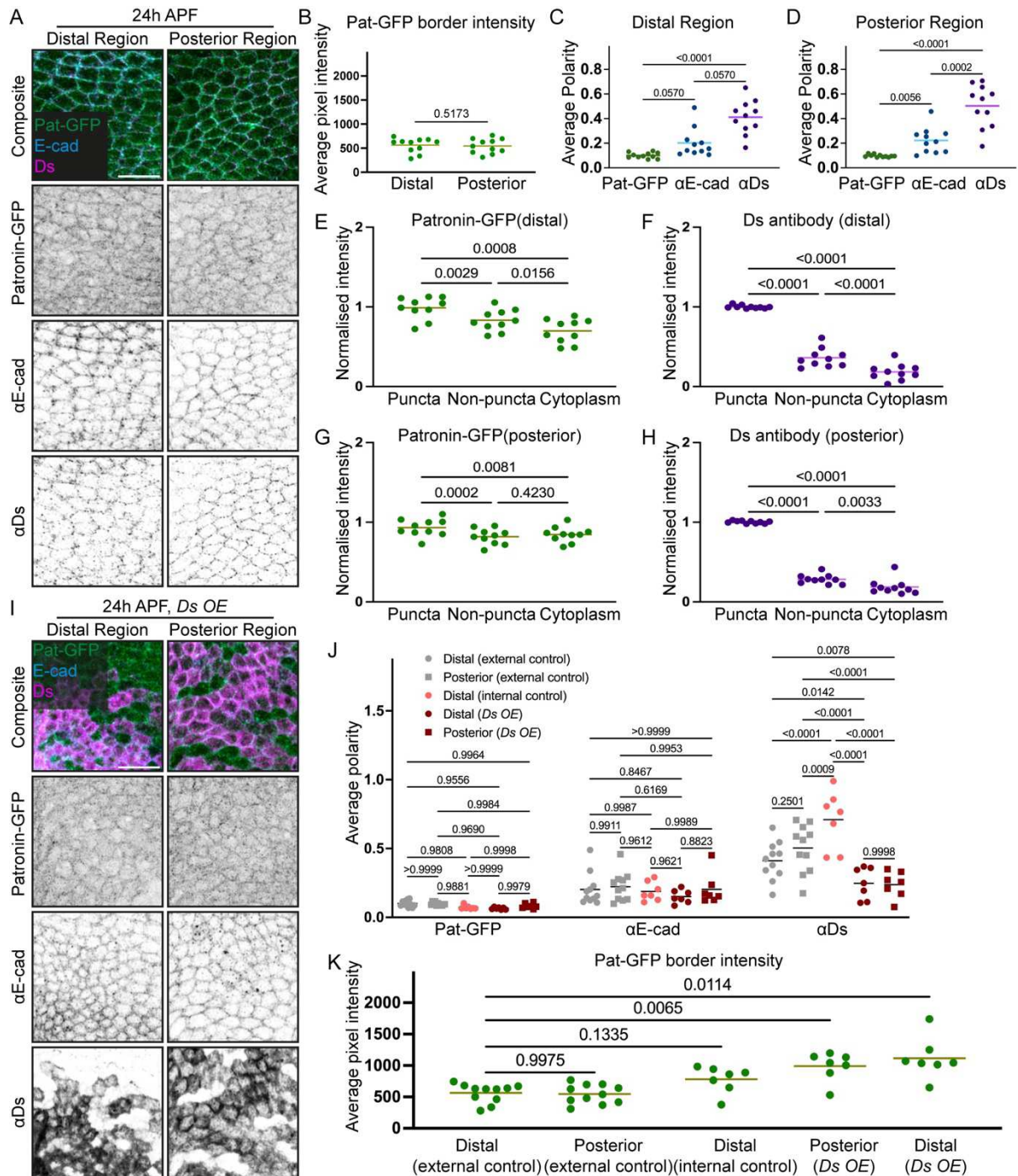
Figure 6. Patronin is weakly recruited to cell boundaries by Ft-Ds complexes in the pupal wing at 24h APF.

(A) Apical view of pupal wings at 24h APF expressing Patronin-EGFP (Pat-GFP, green, top; inverted greyscale, second row) and stained against E-cadherin (E-cad, cyan, top; inverted greyscale, third row) and Ds (magenta, top; inverted greyscale, bottom) in the distal (left) and posterior (right) regions. Scale bar: 10 µm.

(B) Mean intensity of Patronin-EGFP at cell boundaries in cells from distal and posterior regions of pupal wings with normal levels of Ds at 24h APF. Lines indicate the mean values. Two-tailed paired t-test. N = 11.

(C-D) Average polarity of Patronin-EGFP (Pat-GFP), E-cadherin (E-cad) and Ds in the distal (C) and posterior (D) regions. Friedman test (C) and One-Way ANOVA (D) with Dunn's (C) and Tukey's (D) tests for multiple comparisons. N=11 wings.

(E-H) Mean intensity levels of Patronin-EGFP (E, G), and Ds (F, H) at the distal (E, F) and posterior (G, H) regions of the pupal wing, within specific subcellular areas. One-Way ANOVA (E, G, H) and Friedman test (F) and with Tukey's (E, G, H) and Dunn's (F) tests for multiple comparisons. N= 11 wings.

(I) Apical view of pupal wings at 24h APF overexpressing Ds from 18h APF, expressing Patronin-EGFP (Pat-GFP, green, top; inverted greyscale, second row) and stained against E-cadherin (E-cad, cyan, top; inverted grayscale, third row) and Ds (magenta, top; inverted greyscale, bottom) in the distal (left) and posterior (right) regions. Scale bar: 10 µm.

(J) The average polarity of Patronin-EGFP (Pat-GFP), E-cadherin (E-cad) and Ds in the distal and posterior regions with normal Ds levels (external controls), cells without Ds overexpression – adjacent to region with Ds overexpression – in distal regions (internal control) and cells overexpressing Ds (Ds OE) in distal and posterior regions are shown. Two-way ANOVA with Tukey's tests for multiple comparisons. N=11 (external control) and 7 (*Ds OE*) wings.

(K) Mean intensity of Patronin-EGFP at cell boundaries in cells from in the distal and posterior regions with normal Ds levels (external controls), cells without Ds overexpression in distal regions (internal control) and cells overexpressing Ds in distal and posterior regions are depicted. Brown-Forsythe and Welch ANOVA test with Dunnett's T3 test for multiple comparisons. N= 11 (control) and 7 (*Ds OE*) wings. Lines represent the mean values in all graphs.
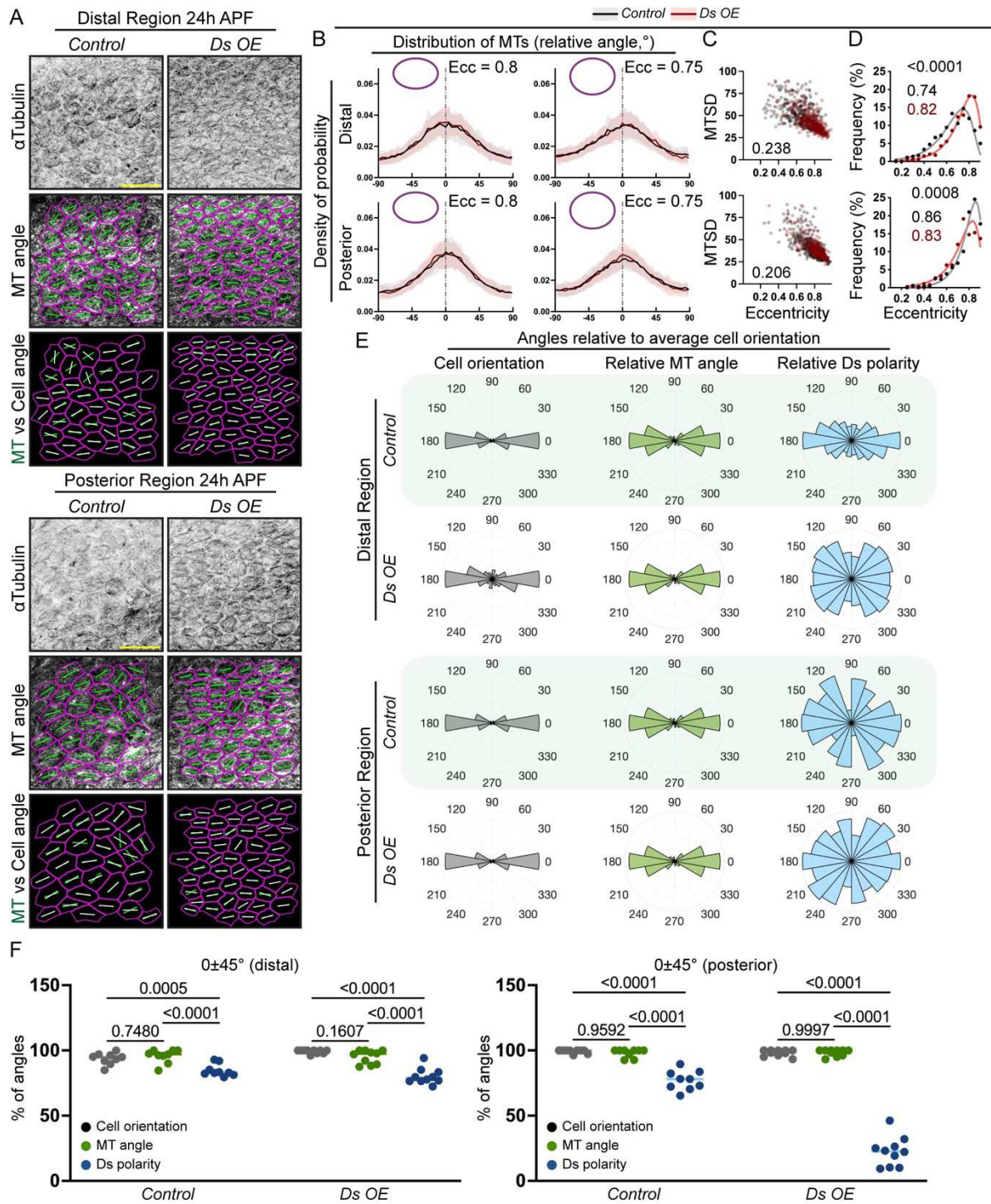
Figure 7. Ds overexpression does not change microtubule organisation at 24h APF.
(A) Apical view of cells in the distal (top group) and posterior (bottom group) regions at 24h APF stained against tubulin (inverted greyscale, top), without (left) or with Ds overexpression (right). Alongside stainings, microtubule angles (green lines, second and bottom rows) and cell angles (white lines, bottom row) are shown. Scale bar: 10 μm.

(B) Microtubule angle distributions (line indicates mean, shading indicates standard deviation) relative to the maximum of the tubulin signal in each cell (0°) binned by cell eccentricity (0.8 ± 0.025, top; 0.75 ± 0.025, bottom) in control cells (black) and cells overexpressing Ds (red) in distal (left) and posterior (right) regions. N= 37 (0.8, distal, control), 42 (0.75, distal, control), 72 (0.8, distal, Ds OE), 52 (0.75, distal, Ds OE), 53 (0.8, posterior, control), 22 (0.75, posterior, control), 46 (0.8, posterior, Ds OE) and 65 (0.75, posterior, Ds OE).

(C) Correlations between MTSD and cell eccentricity at the distal (top) and posterior (bottom) regions, comparing the distributions between control (black) and Ds-overexpressing (red) cells. Each dot represents an individual cell, the numbers indicate p-values for the Pearson's correlations between the two regions tested being different using the bootstrap method. N = 9 (both regions, control) and 10 (both regions, Ds OE).

(D) Distributions of cell eccentricities in control cells (black) or cells overexpressing Ds (red) in the distal (top) and posterior (bottom) regions of pupal wings 24h APF with the binned data points (dots), the best-fit lognormal distributions (lines), the p-value for the probability of the distributions being the same (extra-sum-of-squares F test, black text at top) and modes of the best-fit distributions (black text middle and red text). N = 9 (both regions, control) and 10 (both regions, Ds OE).

(E) Polar histograms depicting binned cell orientations (grey), microtubule angles (green), and Ds polarity (blue) relative to the average cell orientation in each region in control cells (first and third rows) and cells overexpressing Ds (second and bottom rows) in distal (top two rows) and posterior (bottom two rows) regions of pupal wings at 24h APF. N = 9 (both regions, control) and 10 (both regions, Ds OE).

(F) Percentage of angles in the 0±45° range relative to the average cell orientation for cell orientation, microtubule angle and Ds polarity. Lines represent the mean values. One-way ANOVA with Dunn's multiple comparisons test. N= 9 (both regions, control) and 10 (both regions, Ds OE).
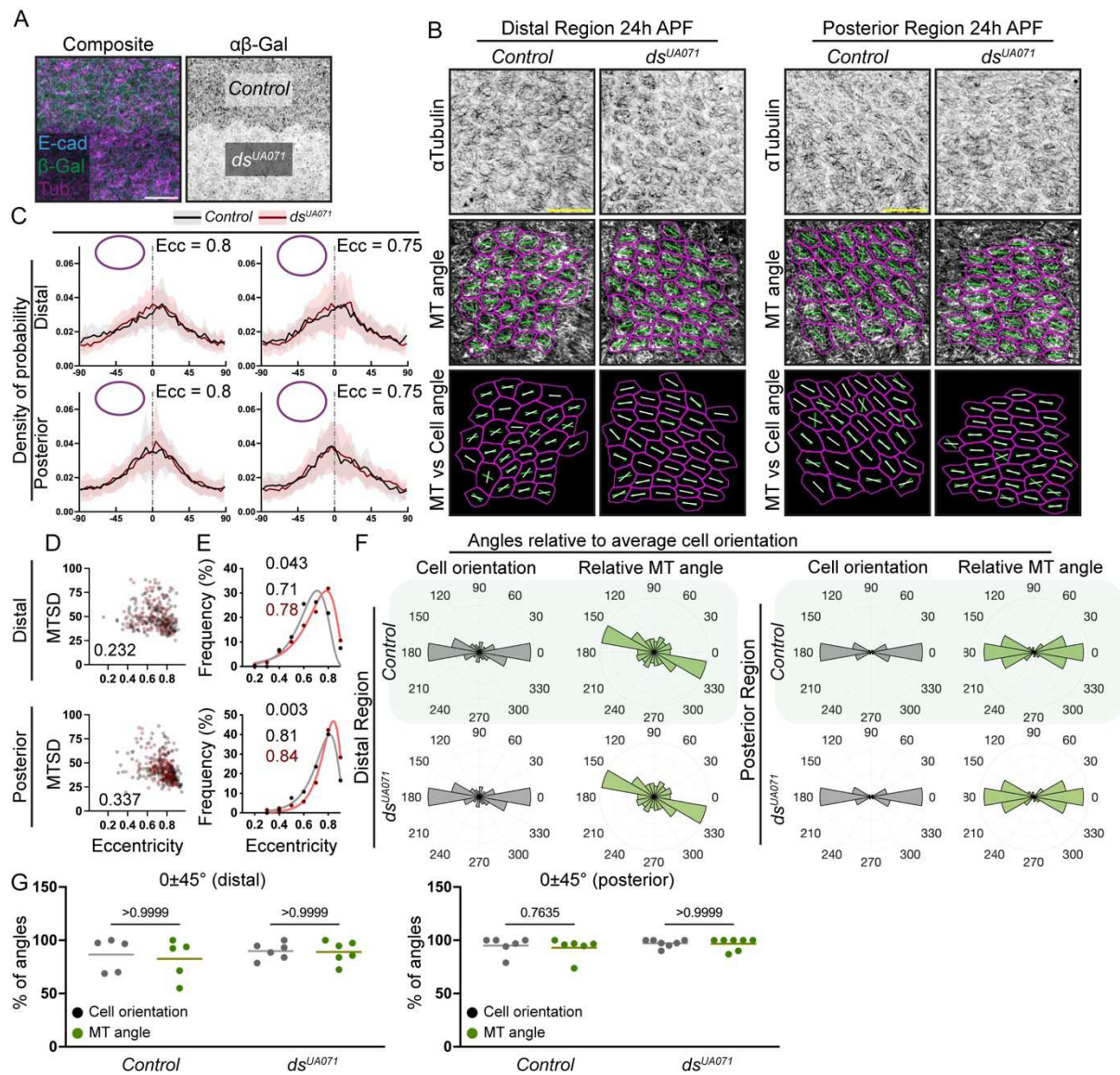
Figure 8. Microtubule organisation does not change in *ds* mutant tissue at 24h APF.

(A) Representative apical views of a clonal border in the posterior region of a pupal wing at 24h APF stained against β-Galactosidase (green, left; inverted greyscale right) whose absence indicates the strong mutant *ds^UA071^/ds^UA071^* clone tissue. Staining against E-cadherin (E-cad, blue) and tubulin (Tub, magenta) are shown on the left. Scale bar: 10 μm.

(B) Apical view of cells in the distal (top group) and posterior (bottom group) regions at 24h APF stained against tubulin (inverted greyscale, top) in control (left) or *ds^UA071^* mutant cells (right). Microtubule angles (green lines, second and bottom rows) and cell angles (white lines, bottom row) are shown. Scale bar: 10 μm.

(C) Microtubule angle distributions (line indicates mean, shading indicates standard deviation) relative to the maximum of the tubulin signal in each cell (0°) binned by cell

eccentricity (0.8 ± 0.025, left; 0.75 ± 0.025, right) in control (green) and ds^{UA071} mutant cells (red) in distal (top) and posterior (bottom) regions. N= 16 (0.8, distal, control), 18 (0.75, distal, control), 24 (0.8, distal, ds^{UA071}), 16 (0.75, distal, ds^{UA071}), 27 (0.8, posterior, control), 19 (0.75, posterior, control), 21 (0.8, posterior, ds^{UA071}) and 26 (0.75, posterior, ds^{UA071}).

(D) Correlation between MTSD and cell eccentricity at the distal (top) and posterior (bottom) regions, comparing the distributions between control (black) and ds^{UA071} (red) mutant cells. Each dot represents an individual cell, the numbers indicate p-values for the Pearson's correlations between the two regions tested being different using the bootstrap method. N = 5 (distal, control), 6 (distal, ds^{UA071}), 6 (posterior, control) and 7 (distal, ds^{UA071}).

(E) Distributions of cell eccentricities in control (black) or ds^{UA071} mutant cells (red) in the distal (top) and posterior (bottom) regions of pupal wings 24h APF with the binned data points (dots), the best-fit lognormal distributions (lines), the p-value for the probability of the distributions being the same (extra-sum-of-squares F test, black text top) and modes of the best-fit distributions (black text middle and red text). N = 5 (distal, control), 6 (distal, ds^{UA071}), 6 (posterior, control) and 7 (distal, ds^{UA071}).

(F) Polar histograms depicting binned and cell orientations (grey) and microtubule angles (green) relative to the average cell orientation in each region in control (top rows) and ds^{UA071} mutant cells (bottom rows) in distal (left two columns) and posterior (right two columns) regions of pupal wings at 24h APF. N = 5 (distal, control), 6 (distal, ds^{UA071}), 6 (posterior, control) and 7 (distal, ds^{UA071}).

(G) Percentage of angles in the 0±45° range relative to the average cell orientation for cell orientation, microtubule angle and Ds polarity. One-way ANOVA with Dunn's multiple comparisons test. Lines represent the mean values. N = 5 (distal, control), 6 (distal, ds^{UA071}), 6 (posterior, control) and 7 (distal, ds^{UA071}).